ARMY RESEARCH LABORATORY

The Effect of Strike Face Geometry on the Dynamic Delamination of Composite Back Plates

by Shane D Bartus and Jacqueline T Le

ARL-TR-7164 **January 2015**

NOTICES

Disclaimers

The findings in this report are not to be construed as an official Department of the Army position unless so designated by other authorized documents.

Citation of manufacturer's or trade names does not constitute an official endorsement or approval of the use thereof.

Destroy this report when it is no longer needed. Do not return it to the originator.

Army Research Laboratory
Aberdeen Proving Ground, MD 21005-5066

ARL-TR-7164 **January 2015**

The Effect of Strike Face Geometry on the Dynamic Delamination of Composite Back Plates

Shane D Bartus and Jacqueline T Le
Weapons and Materials Research Directorate, ARL

REPORT DOCUMENTATION PAGE	Form Approved OMB No. 0704-0188

1. REPORT DATE *(DD-MM-YYYY)*	2. REPORT TYPE	3. DATES COVERED (From - To)
January 2015	Final	June 2013

4. TITLE AND SUBTITLE	5a. CONTRACT NUMBER
The Effect of Strike Face Geometry on the Dynamic Delamination of Composite Back Plates	W911NF-10-2-0076
	5b. GRANT NUMBER
	5c. PROGRAM ELEMENT NUMBER
6. AUTHOR(S)	5d. PROJECT NUMBER
Shane D Bartus and Jacqueline T Le	5e. TASK NUMBER
	5f. WORK UNIT NUMBER
7. PERFORMING ORGANIZATION NAME(S) AND ADDRESS(ES)	8. PERFORMING ORGANIZATION REPORT NUMBER
US Army Research Laboratory ATTN: RDRL-WMP-E Aberdeen Proving Ground, MD 21005-5066	ARL-TR-7164
9. SPONSORING/MONITORING AGENCY NAME(S) AND ADDRESS(ES)	10. SPONSOR/MONITOR'S ACRONYM(S)
George Washington University 2121 I Street NW Washington, DC 20052	GWU
	11. SPONSOR/MONITOR'S REPORT NUMBER(S)

12. DISTRIBUTION/AVAILABILITY STATEMENT

Approved for public release; distribution is unlimited.

13. SUPPLEMENTARY NOTES

14. ABSTRACT

Ceramics are often employed as a hard strike face in composite armor systems. The ceramic serves to break up and erode the penetrator while the back plate absorbs the kinetic energy of the remaining penetrator material. In this program, soda lime glass was used as a surrogate for ceramic to investigate how the strike face geometry affects composite back plate delamination. Understanding how the strike face design influences damage in the armor is an important consideration for multihit requirements. The test specimens were composed of a soda lime float-glass strike face that was adhered to an S-2 glass composite back plate using a transparent adhesive. A 0.30-cal. fragment-simulating projectile was used to ballistically interrogate the specimens, thereby introducing areas of delamination in the backing plate. The inherent translucency of the test specimen allowed for capture of dynamic delamination images with high-speed photography. The projected delamination area was quantified using commercially available digital image analysis software. The effects of glass thickness, geometry, and hit location were studied. It was found that an increase in the strike face diameter resulted in an increase in delamination area and an increase in delamination growth velocity. It was also found that projectile impacts at seam locations between 2 tiles result in more delamination than projectile impacts on the tile center or triple point of the strike faces. These are significant results because they run counter to some of the commonly held beliefs in the armor community.

15. SUBJECT TERMS

composite, armor, ballistic, delamination, ceramic

16. SECURITY CLASSIFICATION OF:			17. LIMITATION OF ABSTRACT	18. NUMBER OF PAGES	19a. NAME OF RESPONSIBLE PERSON
a. REPORT	b. ABSTRACT	c. THIS PAGE			Shane D Bartus
Unclassified	Unclassified	Unclassified	UU	52	19b. TELEPHONE NUMBER (*Include area code*) 410-278-6012

Standard Form 298 (Rev. 8/98)
Prescribed by ANSI Std. Z39.18

Contents

List of Figures

List of Tables

Acknowledgments

We would like to thank Matthew Burkins and Patrick Swoboda for supporting this program. We would also like to thank Donald Little, David Churn, and Phil Davis for aiding in execution of this program. Thanks go to Parimal Patel and Terrence Taylor for donating the glass and to Jim Wolbert who fabricated our targets. Sincere appreciation goes to James Sands and Mick Maher for cost sharing on the target processing in support of the Science and Engineering Apprenticeship Program/College-Qualifed Leaders program. In addition, we would like to thank Dr Sandy Young and George Washington University for contract support.

INTENTIONALLY LEFT BLANK.

1. Introduction

The US Army has a long history in striving for lighter and stronger materials for armor applications. A little more than a decade ago, an Army-wide strategic research objective known as Armor Materials by Design began (Fink 2000). For many applications, even a modest 5%–10% weight reduction is a considerable improvement. Highly mass-efficient armors for small-caliber defeat consist of a ceramic strike face in conjunction with a high-performance composite back plate. One of the inherent weaknesses of such designs is the susceptibility to delamination in the composite back plate, which can degrade multihit performance.

2. Literature Review

Research into the performance of ceramic/composite armor systems began in earnest in the late 1960s. The ceramic is used to break apart and erode the projectile while a composite backing plate supports the ceramic and absorbs the remaining kinetic energy of the projectile fragments (Medvedovski 2010). Ceramic fracture is introduced by tensile, shear, and compressive wave loading (Fink 2000). Typically, the longer a projectile interacts with the ceramic, the more likely it will be defeated (Fink 2000; Hauver et al. 2005). High-performance engineered ceramics can defeat a projectile before it is able to penetrate through to the backing (Hauver et al. 2005). This phenomenon is commonly referred to as interface defeat. However, interface defeat is more an exception than a rule and depends on the prestress state of the ceramic as well as its relative thickness compared with the penetrator diameter, back plate support, and penetrator type and velocity.

The ceramic and soda lime float glass (simply referred to as glass hereafter) used in this study are both brittle materials and behave similarly when impacted by a projectile. However, glasses are amorphous, noncrystalline materials while ceramics are crystalline. Typical ceramics are polycrystalline and contain crystals that are surrounded by a glassy matrix (Bourne 2008). In the present study, glass was used as a ceramic surrogate so that the dynamic delaminations could be visualized experimentally at a significantly lower cost than could be realized using a transparent ceramic such as aluminum oxynitride (AlON).

When glass is impacted by a projectile, a fracture or failure wave propagates through the material. Behind the wave, the material experiences a delayed failure due to compression, the spall strength reduces to a negligible value, and shear strength is decreased (Bourne et al. 1995; Bourne 2005; Bourne 2008). Within the glass, the failure wave is seen as an opaque front because of the cracks that are created (Forde et al. 2010). The failure wave velocity is slower in a

polycrystalline material than in glass (Bourne 2008). However, an increase in impact velocity will increase the failure wave velocity up to a limit dictated by the material properties of the transmission material (Bourne et al. 1995; Anderson et al. 2008). The compressive waves travel through the glass away from the projectile while relief waves travel toward the projectile (Bouzid et al. 2001). Fragmentation of the glass occurs when the relief waves reflect and interact with one another (Bouzid et al. 2001).

Within both glasses and ceramics, a cone or conoid will form when a projectile strikes the material (Madhu et al. 2005; Forde et al. 2010). In the case of the glass, the cone is called a Hertzian cone, named after its discoverer, Heinrich Rudolf Hertz (Forde et al. 2010). The cone is formed when a load is sustained after impact. Upon reflection of the stress/shock waves, the resulting tensile stress creates a crack around the contact area of the projectile. When the load is sustained, the crack becomes a cone and propagates into the surrounding material (Forde et al. 2010).

Within ceramics, the cone typically forms after the projectile tip is destroyed (Madhu et al. 2005). Tension causes axial cracks to form. Radial cracks can propagate from the bottom of the ceramic. Also, there is an increase in shear and spall cracks. The area directly under the projectile is crushed (Madhu et al. 2005), while the top of the cone is flat if there is a backing behind the ceramic (Zuogang et al. 2010).

In many cases, Kevlar, S-2 glass, ultra-high-molecular-weight polyethylene, or a similar high-performance composite laminate is used as the strike face backing or “backer”. The latter will be the focus in this report.

Woven fabrics have interlacing fibers that go over and under, similar to a basket weave (Kim and Sham 2000).This construction gives the fabric a high yarn density, which is an advantage over other weaves. Woven fabrics also have better fracture toughness than unidirectional and cross-ply laminates (Kim and Sham 2000). However, a woven fabric has limited conformability, poor in-plane shear resistance, and reduced tensile and compressive properties (Kim and Sham 2000).

When a projectile hits the fabric, the yarns that the projectile hits become highly stressed (Cheeseman and Bogetti 2003). The yarns in direct contact with the projectile are called primary yarns and provide the resistive force against the projectile (Naik et al. 2006). The yarns that intersect the primary yarns are called secondary yarns (Cheeseman and Bogetti 2003). Transverse and longitudinal waves move through the fabric when the projectile hits the target (Cheeseman and Bogetti 2003). The transverse waves move in the direction that the projectile was moving. The longitudinal waves move in the direction of the fibers toward the point of impact (Cheeseman and Bogetti 2003). A cone will form in the backing because of the transverse waves (Naik et al. 2006). In thin laminates the cone’s height is equal to the distance that the projectile traveled. The cone continues to form until either the target absorbs all of the energy from the projectile or the projectile penetrates the target (Naik and Shrirao 2004).

If the projectile penetrates the target and has an initial energy greater than the amount the target can absorb, it will break the fibers and go through the fabric (Naik et al. 2006). The projectile will not penetrate the target if the initial energy of the projectile is less than the amount of energy the target can absorb (Naik et al. 2006).

Delaminations occur when the layers of the composite separate, caused by cracks in the matrix that decrease interlaminar strength. There are 3 failure modes for delamination: modes I, II, and III (Kim and Sham 2000). During mode I failure, also known as the opening mode, the material pulls apart. During mode II failure, parts of the material slide past each other and cracks occur in the matrix, causing the fibers to debond from the matrix (Kim and Sham 2000). In mode III failure, the material fails because of torsion and twisting. Dynamic delaminations typically propagate as a mixture of mode I and mode II failures. Delaminations begin where the projectile hits the target and spread outward and occur when critical shear strain is exceeded (Potti and Sun 1996).

Shear plugging can also occur when a projectile hits the target. During shear plugging, part of the target forms a plug that is about the size and shape of the projectile (Bartus 2006). That plug is forced out when the stress in the target around the projectile is greater than the shear plugging strength.

Delaminations can occur without any appreciable penetration (Potti and Sun 1996). The area of delamination depends on the impact velocity, duration of contact, and the propagation of the stress waves. It increases as the velocity of the projectile increases until shear plugging begins and the projectile penetrates. The area of delamination decreases as the velocity of the projectile increases past the minimum velocity needed to penetrate the target. The greatest amount of ballistic damage occurs when a projectile's velocity is just below the $V_{50,}$ the velocity where 50% of the projectiles perforate the material (Resnyansky 2006b).

In addition to cone formation, delamination, and shear plugging, the target absorbs the projectile's energy through its yarns. Energy is absorbed by the primary yarns through tension and by the secondary yarns through elastic deformation, and energy from friction is also absorbed upon impact of the projectile (Naik and Shrirao 2004).

Damage such as delamination is known to decrease the bending stiffness of a material (Hou and Jeronimidis 2000). According to Deluca et al. (1998), delamination increases elastic bending. Large amounts of delamination will increase the local thickening of the damaged area and will actually increase bending stiffness. Bending stiffness affects the ability of a material to support other objects such as a glass or ceramic strike face. It can lead to debonding of the strike face from the back plate, which can adversely affect the subsequent armor performance (Mahd et al. 2003). If compression is added to a delaminated material, that material will structurally fail (Resnyansky 2006a). Once the structure fails, the composite and ceramic will have little effect against a projectile.

3. Experiment

Two similar experiments were conducted to investigate how the geometry of the strike face affects the delamination in composite back plates. In both experiments, targets were created, ballistically interrogated, and analyzed to quantify the damage. The first experiment studied how the thickness and size (area) of the strike face affected delamination, while the second experiment examined the effect of strike face impact location on delamination. The locations examined were the tile center, the seam between 2 tiles, and the triple point between the intersection of 3 tiles.

3.1 Materials

In both experiments, targets were fabricated by adhering soda lime glass to a thin, translucent S-2 glass/SC-15 epoxy backing plate. A 0.30-cal. fragment-simulating projectile (FSP) was used to strike the front of the target, while real-time delamination growth was recorded using a high-speed camera from behind the target.

Float glass was chosen as a surrogate for ceramics because it is more cost effective than ceramic, readily available, and brittle. An advantage to using glass is its transparency, which makes the delaminations visible from the back side of the target. Transparent ceramics such as AlON are expensive because of the high cost of machining and finishing and thus were not used for these experiments (McCauley et al. 2009). An 8-ply $(0,90)_{2S}$, 24-oz/yard, 5 × 5 basket weave AGY S-2 glass/SC-15 epoxy was chosen as the composite backing. Quasi-static material and high strain-rate properties for this composite are well characterized and have been previously reported by Bartus (2006). The 8-ply laminate is thin enough to allow high-intensity white light to pass through. Starphire soda lime float glass was chosen for the strike face because of its optical and ballistic properties. The material properties of the glass, taken from Grujic (2012), are shown in the Table.

Table Mechanical properties of soda lime glass

Property	Symbol	Value	Unit
Young's modulus	E	70.0	GPa
Poisson's ratio	ν	0.22	N/A
Density	ρ	2500	kg/m^3
Surface-controlled fracture			
Weibull modulus	m	7	NA
Mean static fracture strength	$\sigma_{f,static}$	50	MPa
Effective surface	Z_{eff}	0.024	m^2
Volume-controlled fracture			
Weibull modulus	m	30	NA
Mean static fracture strength	$\sigma_{f,static}$	230	Mpa
Effective volume	Z_{eff}	10^{-4}	m^3

3.2 Target Construction

The S-2 glass/SC-15 epoxy back plates were made through the vacuum-assisted resin transfer molding (VARTM) process, during which a glass table was cleaned and coated with Freekote mold release (Bartus 2006). Infusion and extraction tubes for the resin were put into place. The S-2 glass fabric and a release film made out of woven nylon were placed on the table and covered by a vacuum bag. A vacuum was used to draw the resin into the vacuum bag onto the fabric and release film. The samples were then cured at room temperature under a vacuum for 24 h. Then they were cured for an additional 160–170 h at room temperature. Finally, the samples were cured in an oven at 82 °C for 5 h (Bartus 2006). The areal density of the 8-ply laminate is nominally 0.41 $kg{\cdot}m^{-2}$ (2 psf).

The glass was bonded to the S-2 glass/SC-15 epoxy using 0.635 mm of Deerfield Thermoplastic Polyurethane (TPU). First the S-2 glass/SC-15 epoxy laminates were sanded where the glass was to be placed and cleaned with acetone. The glass and TPU were cleaned with isopropyl alcohol. The TPU was cut into the same shape and size as the glass pieces and was sandwiched between the glass and S-2 glass/SC-15 epoxy. There were 2 pieces of glass attached to each composite backing for the targets in the first experiment at sufficient distance such that damage from the first impact would not have any effect of the adjacent impact site. Each piece was placed 17.8 cm from the corner along one of the diagonals of the composite backing. Only one tile configuration was placed on each back plate for the second experiment. The targets were placed in a vacuum bag and placed under vacuum. Later, temperatures were elevated to melt the TPU, which allowed the glass to adhere to the backing. The oven was heated to 121 °C at a ramp of 0.5 °C/min. Then the temperature was held at 121 °C for 3 h. Then the oven was allowed to cool back to room temperature under a vacuum. The oven does not cool at a specific rate (see Fig. 1).

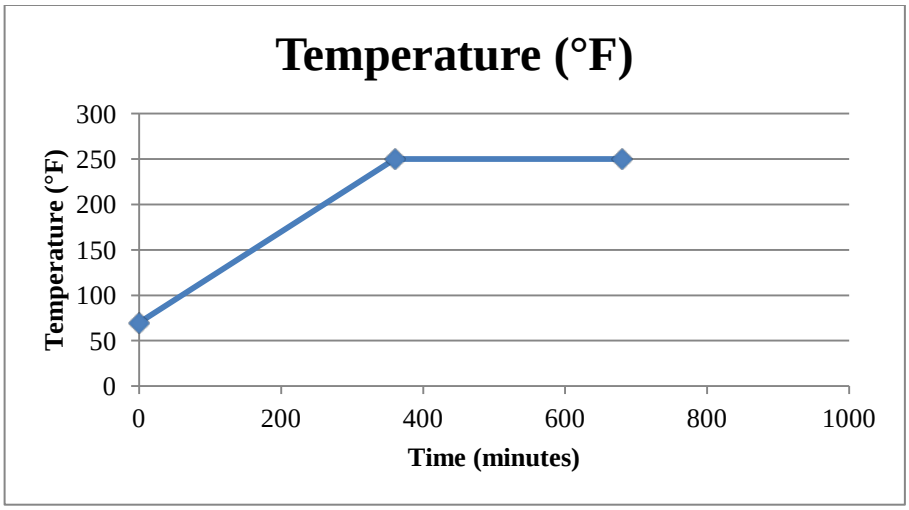

Fig. 1 Heat cycle for targets

For the first experiment, 6 glass targets were made, each set up to be shot twice. There were 2 different thicknesses, 6.0 and 12.7 mm, and 3 different diameters, 25.4, 38.1, and 76.2 mm. There were 2 tiles for each combination of thickness and diameter (see Appendix A for a list of the different targets).

The second experiment consisted of 16 targets. Four targets consisted of one 75- × 75-mm square glass tile mounted to the center of the S-2 glass/SC-15 epoxy back plates. Eight targets consisted of 2 adjacent square glasses centered on the composite back plate. The last 4 targets consisted of 3 square tiles oriented to create a triple point. The square tiles were also centered onto the S-2 glass/SC-15 epoxy back plates (see Figs. 2–4).

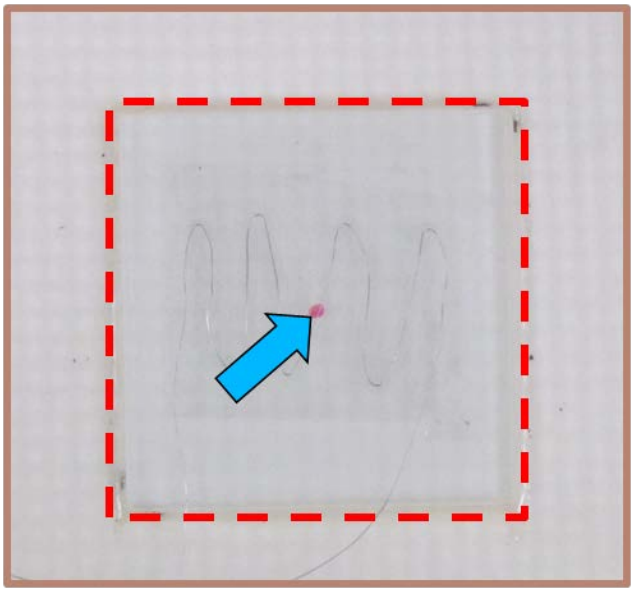

Fig. 2 Center hit target

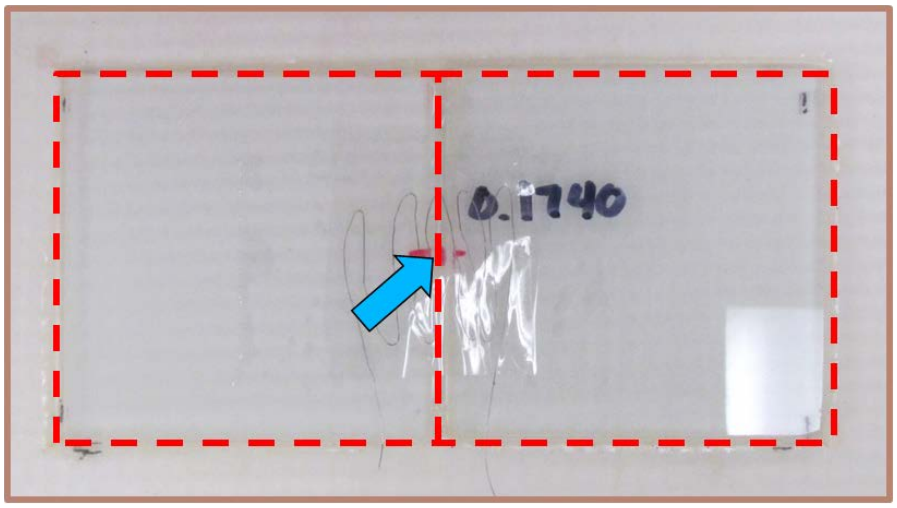

Fig. 3 Two-tile arrangement target

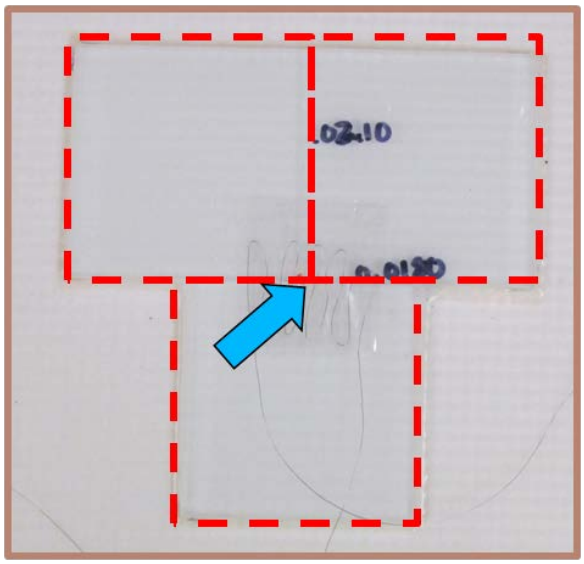

Fig. 4 Triple-point target

3.3 Light Transmission Experiment

Prior to testing the targets, the investigators needed to determine whether the delaminations could be seen through the back plate and broken glass. When the glass fractures, the cracks diffuse some of the light that transmits through the glass and composite backing. Since cracks in soda lime glass travel 3–4 times faster than delaminations, there is potential for blocking the through-thickness light transmission and obscuring the delaminations.

Two blocks of glass were used in a simple experiment. Both pieces of glass were taped with transparent packing tape (Scotch [3M] mailing and storage tape) on both sides. There were 2

layers of tape placed onto each side of the glass. The pieces of tape in the first layer were all placed in the same direction. The second layer of tape was placed perpendicular to the first layer of tape.

The pieces of glass were then laid on the floor and a 141-cm tube was held 4 cm above the glass. A 64.04-g steel rod was dropped onto the glass through a tube to break it. At the time of impact, the rod had 9.1 J of kinetic energy (calculated). The tube ensured that the rod impacted the glass with minimal pitch and yaw. The rod was dropped repeatedly onto different parts of the glass to propagate as many cracks as possible. The rod was dropped 20 times onto the first piece of glass and 37 times onto the second piece of glass. A heavier and denser tungsten rod was used for the last 2 drops onto the second piece of glass.

Although the glass was broken, the tape kept the pieces and fragments together. The broken glass block was taped behind the S-2 glass/SC-15 epoxy, which was placed in front of a light with the glass between the light and the composite. Pictures were taken of the composite from the side without the glass.

The cracks were visible through the S-2 glass/SC-15 epoxy; however, they did not obstruct the light too much. The more visible cracks were areas where a lot of cracks were concentrated together. Most of the cracks were hard to see, which means they would not interfere much with the visibility of the delaminations during the shots and on the high-speed camera footage.

3.4 Ballistics Experimentation

A 0.30-cal. FSP was shot at the targets. A schematic of the Aberdeen Proving Ground, MD, range is shown in Fig. 5. A Model 35 Oehler proof chronograph was used to measure the velocity of the projectile (Model 35P 2011). For the first experiment, the striking velocity was 500 m/s for the 6-mm-thick glass and 750 m/s for the 12-mm-thick glass. The striking velocity for the second experiment was 500 m/s for all of the targets.

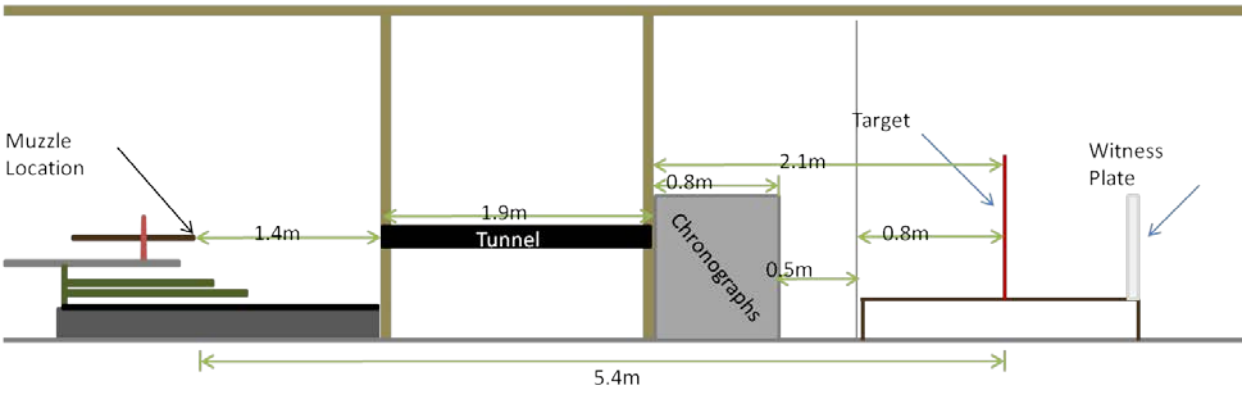

Fig. 5 Test range setup

A light bank was used to illuminate the side of the target that was struck by the projectile. A mirror was set up behind the target to reflect the back of the target to the high-speed camera that recorded the growth of delaminations.

3.5 Analysis

The images from the high-speed camera were analyzed using Image Pro Plus version 6.3 (Appendix B). The area of delamination was measured as a function of time. Post-impact pictures were used to measure the total area of delamination. The colors and contrast of the picture were adjusted to see the delaminations more clearly, and the polygon tool was used to trace and measure the area of delamination. There was a problem with keeping consistency while tracing the delaminations. In most cases, delaminating occurred in a “reverse Christmas tree” pattern throughout the laminate, and it was difficult to distinguish the outermost layer of delamination.

The velocity of the growth of delamination was measured using Phantom version 640. The images from the high-speed camera footage were used to measure the velocity. Two points were selected in 2 consecutive frames, and the program used the scale and time to measure the distance between the 2 points and obtain the velocity. The 2 points chosen were on the edge of the delamination and showed how the delamination grew. For the second experiment, the velocity was measured along the primary and secondary yarns.

4. Results and Discussion

4.1 Effects of Size and Thickness

The targets were shot and post-impact pictures were taken. The results are given in Figs. 6–13. The high-resolution post-impact images were used to measure the area of delamination and can be found in Appendix C. The delamination measurements for the first experiment are shown in Figs. 6 and 7. The dashed lines indicate the baseline test where the composite back plate was struck at the same velocity as the other tests without a strike face. For a summary of all the areas, diameters, and thicknesses, see Appendix A.

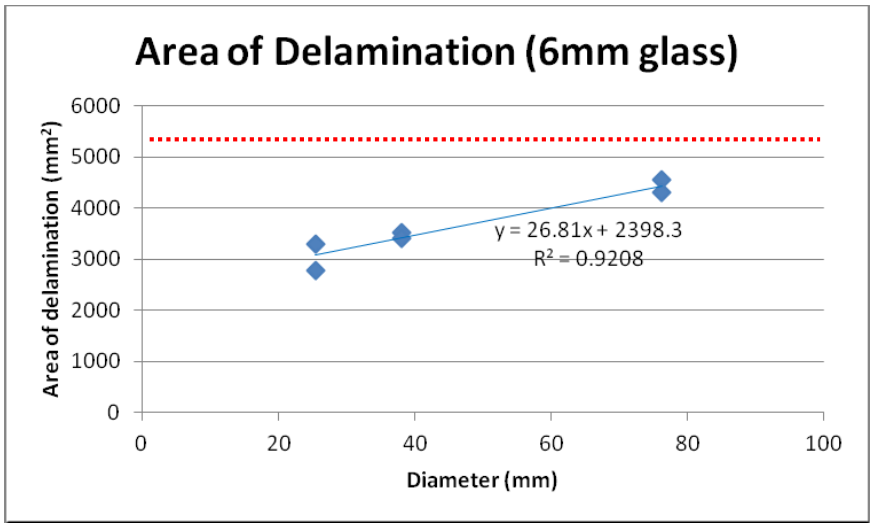

Fig. 6 Area of delamination vs. tile diameter for the 6-mm-thick glass shot at nominally 500 m/s

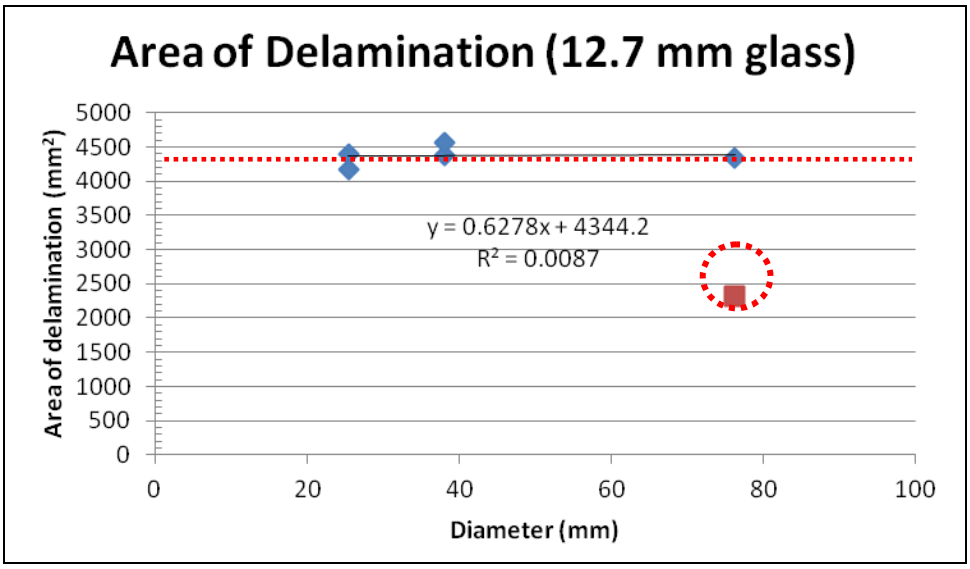

Fig. 7 Area of delamination vs. tile diameter for the 12.7-mm-thick glass shot at nominally 750 m/s. The circled point is the pseudo safety glass that had been taped on one side.

The initial test plan was to shoot at the targets at a constant velocity of 500 m/s. However, the first impact at 500 m/s on the 12.7-mm-thick glass resulted in no appreciable delamination, so the striking velocity had to be increased to 750 m/s. This striking velocity would have been likely to result in a complete penetration for the thinner 6-mm-thick strike face specimens, so the impact velocity for those targets was kept at 500 m/s. As a result, the effect of strike face thickness could not be directly compared. However, for both strike face thicknesses, the effect of diameter was compared and 2 distinct results were obtained, as shown in Figs. 6 and 7.

In Fig. 6, there is a linear trend showing that the delamination area increased for the 6-mm glass as the diameter of the glass increased. Since no additional specimens and diameters were tested, it cannot be concluded whether or not there is a plateau where the diameter will increase but the area of delamination will not. In Fig. 7, there appears to be a plateau showing that with the 12.7-mm glass, the area of delamination was not dependent on the diameter of the glass. It is interesting to see that with the 6-mm-thick glass, which is the about same thickness as the back plate, diameter does have an effect on the area of delamination, whereas with the 12.7-mm-thick glass, which is about twice as thick as the back plate, diameter does not have an effect on the area of delamination.

There is some bias with the second 12.7-mm-thick, 76.2-mm-diameter sample that was shot. That shot resulted in 2,316 mm^2 of delamination, but the glass was a pseudo safety glass (2 layers of transparent packing tape on the strike face). The side of the glass that was struck had 2 layers of tape to contain the fragments and to reduce the debris cloud. While the cracks in the glass did not block the through transmission of light, the debris cloud did. For some of the tests, especially for the 12.7-mm-thick glass, it was hard to see and distinguish the delamination growth in the high-speed camera footage. The delamination velocity was not reported in the cases where it could not be accurately measured, but the delamination area was always reported. Figure 8 shows the area of the delamination in representative test specimens as a function of time. The area of delamination grows with time, but the velocity of growth slows over time. It appears that as the diameter for the 6-mm-thick glass increases, the change in the velocity of the delamination growth becomes more linear. Representative images of delamination growth for the 6-mm-thick, 38.1-mm-diameter strike face are shown in Appendix D. The velocity was measured along both the primary and secondary yarns (see Fig. 9). For both thicknesses, the velocity of the delamination growth increased as the diameter of the strike face increased.

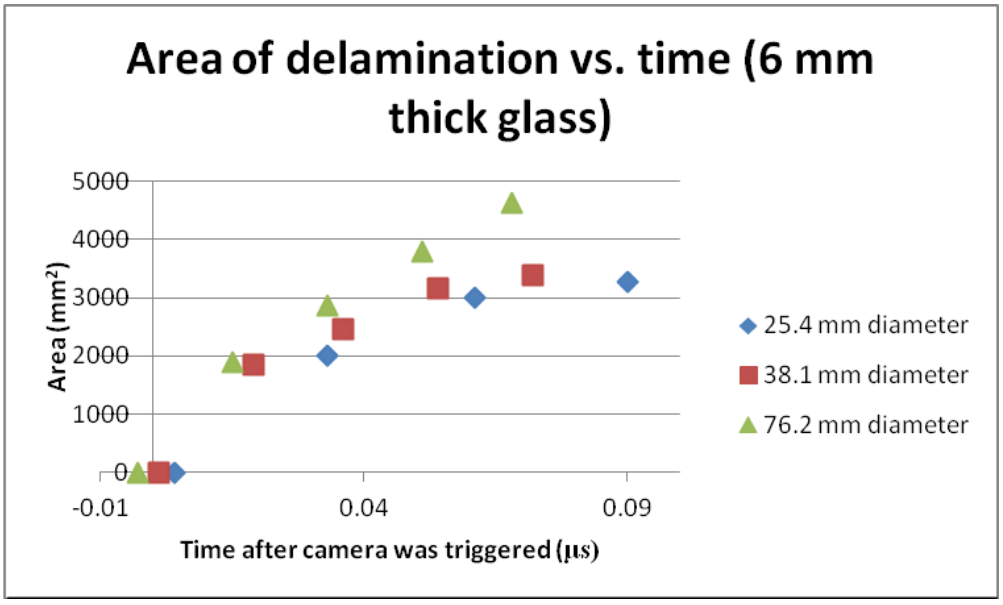

Fig. 8 Area of the delamination as a function of time for the 3 tile diameters

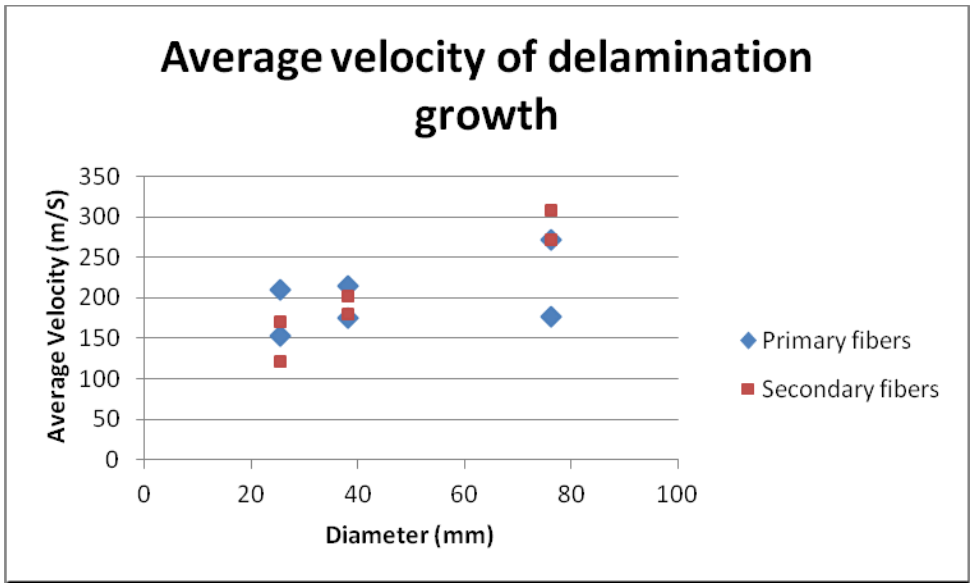

Fig. 9 Average velocity of delamination growth in both primary and secondary yarns vs. tile diameter

In general, the velocity of growth decreased over time. (Further analysis of the delamination growth velocity is given in Appendixes E and F.) However, there are some samples where this was not the case (see Appendix C, Fig. C-1). The increase in growth rate instead of a decrease may be the result of difficulties in distinguishing between delamination and debris. The sudden increase in velocity may also be attributed by a change in the mode of damage from opening to sliding or bending mode.

4.2 Effect of Hit Location

For the second experiment, all of the targets were shot with a 0.30-cal. FSP at 500 m/s. Again, high-speed camera footage and post-impact pictures were used to analyze the data. To address the problem of the debris cloud, a lens was set up to magnify the light used to illuminate the target. The magnified light had a greater intensity than just the bank of light and was able to pass through the debris cloud to illuminate the delaminations.

Along all yarns, the 2-tile seam-impact arrangement had the fastest delamination growth velocity. Figs. 10, 11, and 12 show that the delamination velocity for 2-tile arrangements grew on average at 330 m/s along the primary yarns and 334 m/s along the secondary yarns. The graphs also show that the triple points had the next fastest delamination growth velocity, which grew on average at 280 m/s along the primary and secondary yarns or about 15% slower than the velocity for the 2-tile arrangements. The center had the slowest delamination growth velocity. The delamination of the center hits grew on average at 265 m/s along the primary yarns and 241 m/s along the secondary yarns, which is about 20% slower than the velocity for the 2-tile arrangement.

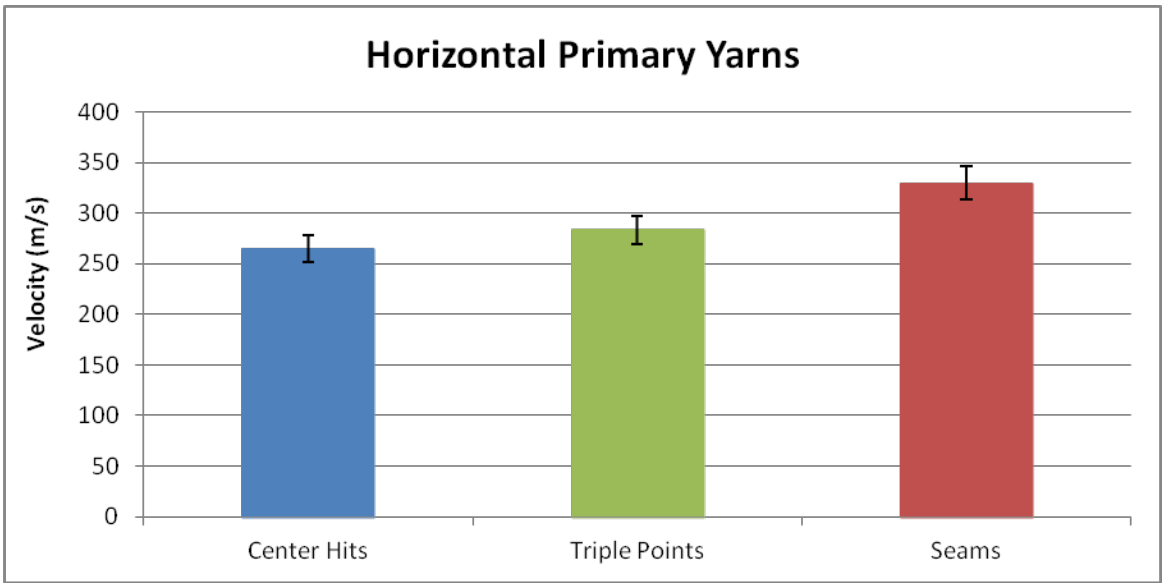

Fig. 10 Average delamination velocities along the primary horizontal yarns

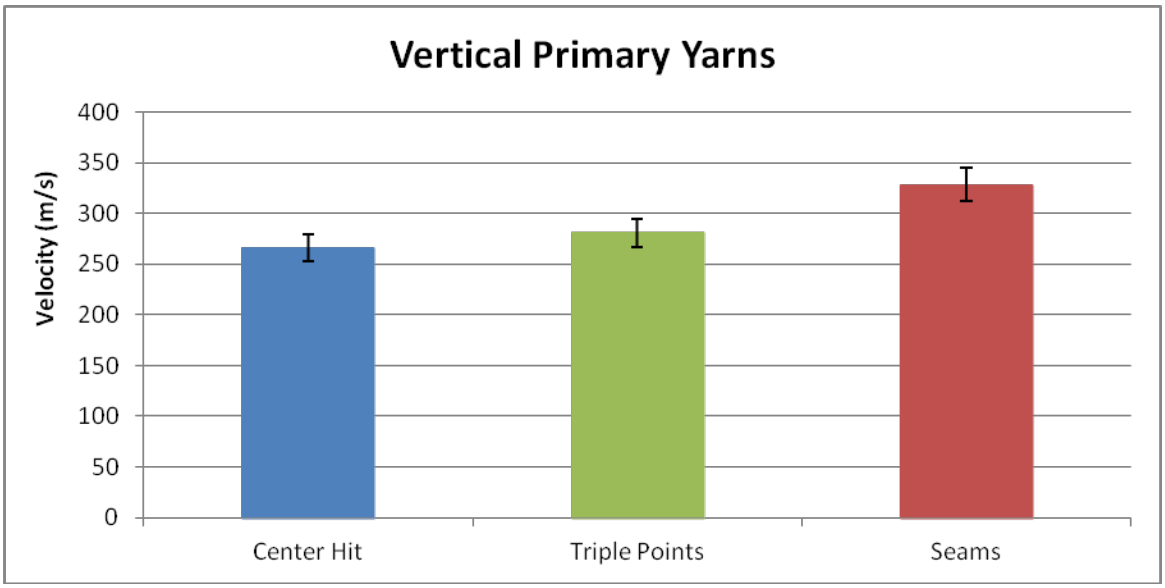

Fig. 11 Average delamination velocities along the primary vertical yarns

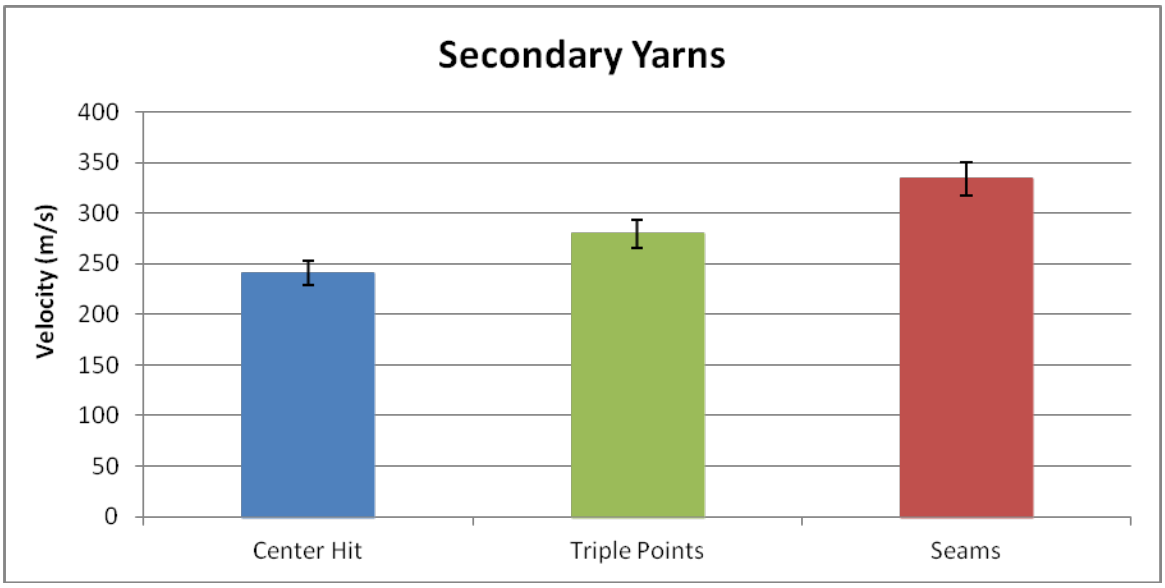

Fig. 12 Average delamination velocities along the secondary yarns

Figs. C-2, C-3, and C-4 in Appendix C are typical examples showing delamination for center, seam, and triple-point impacts, respectively. The dark areas in the figures are the areas that were measured. Fig. 13 shows that the triple points had the largest area of delamination with an average of 0.0060 m^2. The 2-tile arrangements had an area of delamination of 0.0051 m^2, and the center hits had an area of delamination of 0.0050 m^2, which are 15% and 17% smaller than the area of delamination of the triple points, respectively. The differences between the areas of delamination of the 2-tile arrangements and center hits were insignificant.

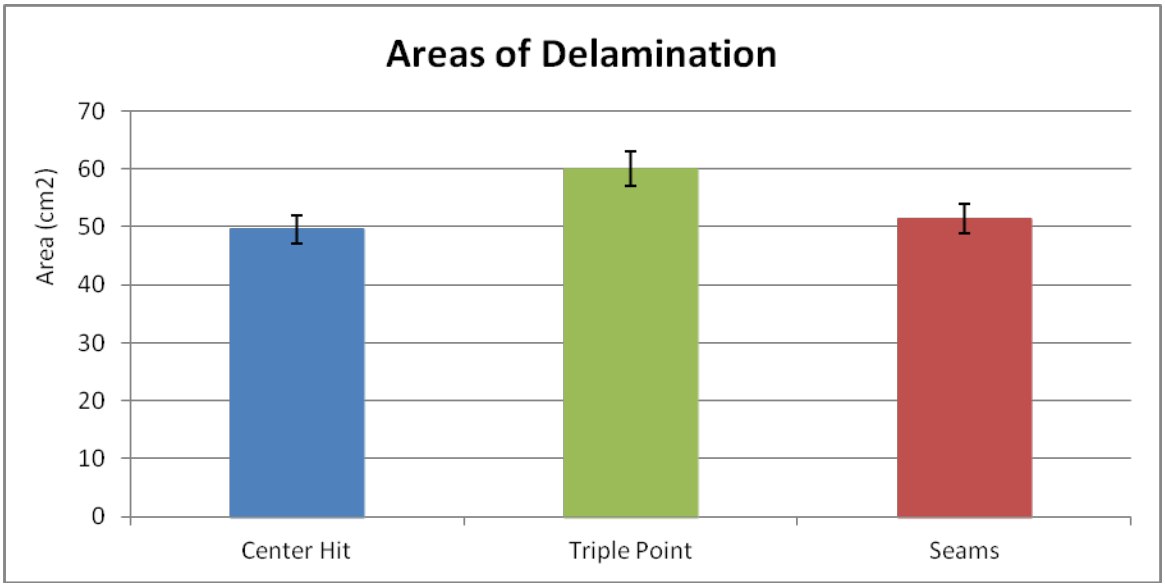

Fig. 13 Average areas of delamination

Any errors in the data may be from problems that occurred during the construction of the targets. For 2 of the 2-tile arrangements, the Deerfield Thermoplastic Polyurethane pieces were cleaned with acetone, which degrades it. Another problem was one 2-tile arrangement had a very large gap between the 2 tiles. However, there were not any obvious outliers in the data despite these mistakes in target construction.

5. Conclusions

The effect of geometry of strike faces and the hit location on the delamination of composite back plates were investigated. It was found in some cases that the geometry of the strike face does affect delamination. There was a linear relationship between delamination area and glass diameter for the 6-mm-thick glass but not the 12.7-mm-thick glass. For both thicknesses, the delamination growth velocity increased as the diameter of the glass increased. For the 6-mm-thick glass, the change in the velocity of the growth of delamination becomes more linear as the diameter increases.

To determine whether thickness has an effect on the area of delamination, it is suggested that the V_{50} be found to select an appropriate velocity that would cause a partial penetration and still initiate delamination in multiple thicknesses of glass.

The hit location also affects the delamination of the composite back plate. The 2-tile arrangement had the fastest delamination growth velocity, while the single tile arrangement had the slowest. The triple-point targets had the largest average area of delamination while the single tile arrangement had the smallest average area of delamination.

Future research and development should focus on the seams (2-tile arrangement) and the triple points to reduce the delamination growth velocity and delamination area respectively. More research should be done to find the optimal ceramic tile geometry that maximizes protection and minimizes weight, material, and associated manufacturing costs. This work may serve as a rapid method of assessing composite back plate designs in addition to gaining a better understanding of the strike face design parameters.

6. References

Anderson CE, Chocron S, Bigger RP. Time-resolved penetration into glass: experiments and computations. International Journal of Impact Engineering. 2008;38(8–9):723–731.

Bartus SD. Simultaneous and sequential multi-site impact response of composite laminates. [dissertation]. [Birmingham (AL)]: The University of Alabama at Birmingham; 2006.

Bourne NK. On the impact and penetration of soda lime glass. International Journal of Impact Engineering. 2005;32(1–4):65–79.

Bourne NK. The relation of failure under 1D shock to the ballistic performance of brittle materials. International Journal of Impact Engineering. 2008;35(8):674–683.

Bourne NK, Rosenberg Z, Field JE. High-speed photography of compressive failure waves in glass. Journal of Applied Physics. 1995;78(6):3736–3739.

Bouzid S, Nyoungue A, Azarl Z, Bouaouadja N, Pluvinage G. Fracture criterion for glass under impact loading. International Journal of Impact Engineering. 2001;25(9):831–845.

Cheeseman BA, Bogetti TA. Ballistic impact into fabric and compliant composite laminates. Composite Structures. 2003;61(1–2):61–173.

DeLuca E, Prifti J, Bethaney W, Chou SC. Ballistic impact damage of S-2 glass-reinforced plastic structural armor. Composite Sciences and Technology. 1998;58(9):1453–1461.

Fink BK. Performance metrices for composite integral armor. Journal of Thermoplastic Composite Materials. 2000;13(5):417–431.

Forde LC, Proud WG, Walley SM, Church PD, Cullis IG. Ballistic impact studies of a borosilicate glass. International Journal of Impact Engineering. 2010;37(5):568–578.

Grujicic M, Bell WC, Pandurangan B. Design and material selection guidelines and strategies for transparent armor systems. Materials & Design. 2012;34:808–819.

Hauver GE, Rapacki EJ Jr, Netherwood PH, Benck RF. Interface defeat of long-rod projectiles by ceramic armor. Aberdeen Proving Ground (MD): Army Research Laboratory (US); 2005 Sep. Report No.: ARL-TR-3590.

Hou JP, Jeronimidis G. Bending stiffness of composite plates with delamination. Composites Part A: Applied Science and Manufacturing. 2000;31(2):121–132.

Kim JK, Sham ML. Impact and delamination failure of woven-failure of woven-fabric composites. Composite Science and Technology. 2000;60(5):745–761.

Madhu V, Ramanjaneyulu K, Balakrishna Bhat T, Gupta NK. An experimental study of penetration resistance of ceramic armour subjected to projectile impact. International Journal of Impact Engineering. 2005;32(1–4):337–350.

Mahd S, Gama BA, Yarlagadda S, Gillespie JW. Effect of the manufacturing process on the interfacial properties and structural performance of multi-functional composite structures. Composites Part A: Applied Science and Manufacturing. 2003;34(7):635–647.

McCauley JW, Patel P, Chen M, Gilde G, Strassburger E, Paliwal B, Dandekar DP. AlON: A brief history of its emergence and evolution. Journal of the European Ceramic Society. 2009;29:223–236.

Medvedovski E. Ballistic Performance of armour ceramics: influence of design and structure. part 1. Ceramics International. 2010;36(7):2103–2115.

Model 35P. [accessed 2011] from http://www.oehler-research.com/model35p.html.

Naik NK, Shrirao P. Composite structures under ballistic impact. Composite Structures. 2004;66(1–4):579–590.

Naik NK, Shrirao P, Reddy, BCK. Ballistic impact behaviour of woven fabric composites: formulation. International Journal of Impact Engineering. 2006;32(9):1521–1552.

Potti SV, Sun CT. Prediction of impact induced penetration and delamination in thick composite laminates. International Journal of Impact Engineering. 1996;19(1):31–48.

Resnyansky AD. The impact response of composite materials involved in helicopter vulnerability assessment: literature review – part 1. Edinburgh (South Australia): Defence Science and Technology Organisation; 2006a. Report No.: DSTO-TR-1842 Part 1.

Resnyansky AD. The impact response of composite materials involved in helicopter vulnerability assessment: literature review – part 2. Edinburgh (South Australia): Defence Science and Technology Organisation; 2006b. Report No.: DSTO-TR-1842 Part 2.

Zuoguang Z, Mingchao W, Shuncheng S, Min L, Zhijie S. Ingluence of panel/back thickness on impact damage behavior of alumina/aluminum armors. Journal of European Ceramic Society. 2010;30:875–887.

INTENTIONALLY LEFT BLANK.

Appendix A. Summary of Shot Data

Tables A-1 and A-2 detail test shot data.

Table A-1 Shot number, thickness and diameter of the glass for each shot, and the area of delamination based on post-impact measurements

Shot No.	Diameter (mm)	Thickness (mm)	Post-impact Area of Delamination (mm^2)
10813	25.4	6	3,302
10814	25.4	6	2,789
10815	38.1	6	3,521
10816	38.1	6	3,409
10817	76.2	6	4,549
10818	76.2	6	4,311
10819	38.1	12.7	4,379
10820	38.1	12.7	4,562
10821	25.4	12.7	4,399
10822	25.4	12.7	4,168
10823	76.2	12.7	4,341
10824	76.2	12.7	2,316 Pseudo safety glass

Table A-2 Shot number, velocities of delamination along each yarn type, and the area of delamination for each shot

Shot No.	Velocity of Delamination			Area of Delamination (cm^2)
	Primary Horizontal (m/s)	Primary Vertical (m/s)	Secondary (m/s)	
Baseline				
11432	186.629	245.907	236.343	51.02489
11433	162.185	224.563	208.479	43.77680
11434	137.106	254.729	216.937	53.47646
11435	156.265	154.609	237.318	49.94783
Seams				
11436				46.87624
11437	156.265	222.061	221.298	47.76642
11438	151.294	138.686	241.367	45.71520
11439	185.607	123.691	211.493	54.55994
11440	189.415	186.97	220.927	63.74364
11441	149.824	174.650	194.258	56.02041
11442	165.582	140.253	212.083	46.50445
11443	193.195	155.846	255.611	52.71091
Triple Points				
11444	204.555	224.567	282.366	59.39147
11445	164.603	189.522	294.153	63.68293
11446	206.291	221.320	260.251	53.49493
11447	…	…	…	63.73810

Appendix B. Select Images from the High-Speed Camera and Image Pro Plus

Figures B-1 through B-3 show software-manipulated imagery

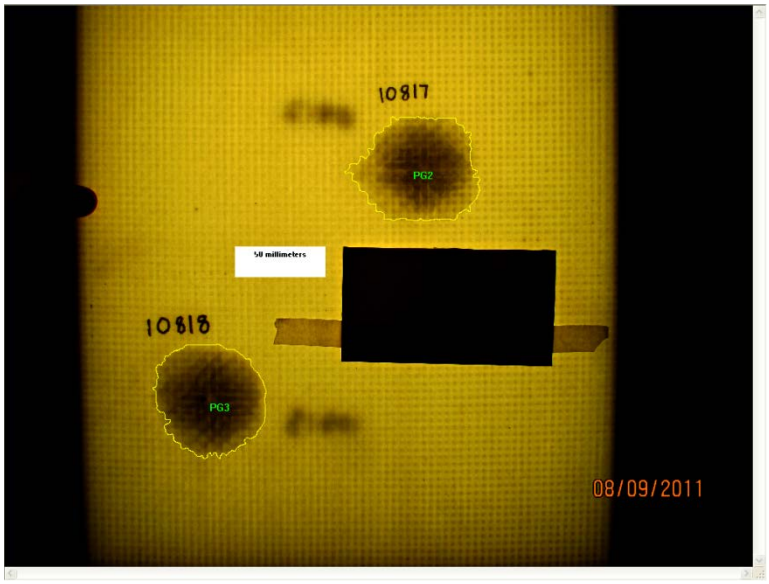

Fig. B-1 Delaminations outlined using tools in Image Pro Plus

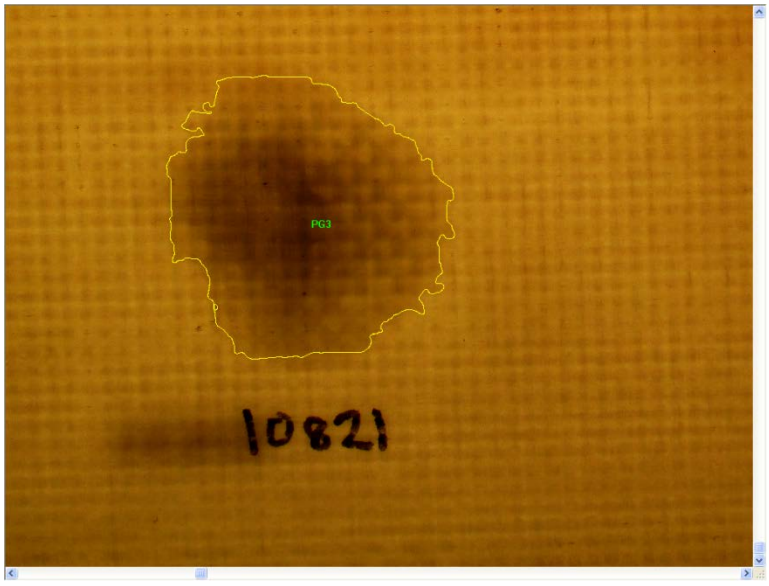

Fig. B-2 Yellow outline indicates delamination area measured with Image Pro Plus

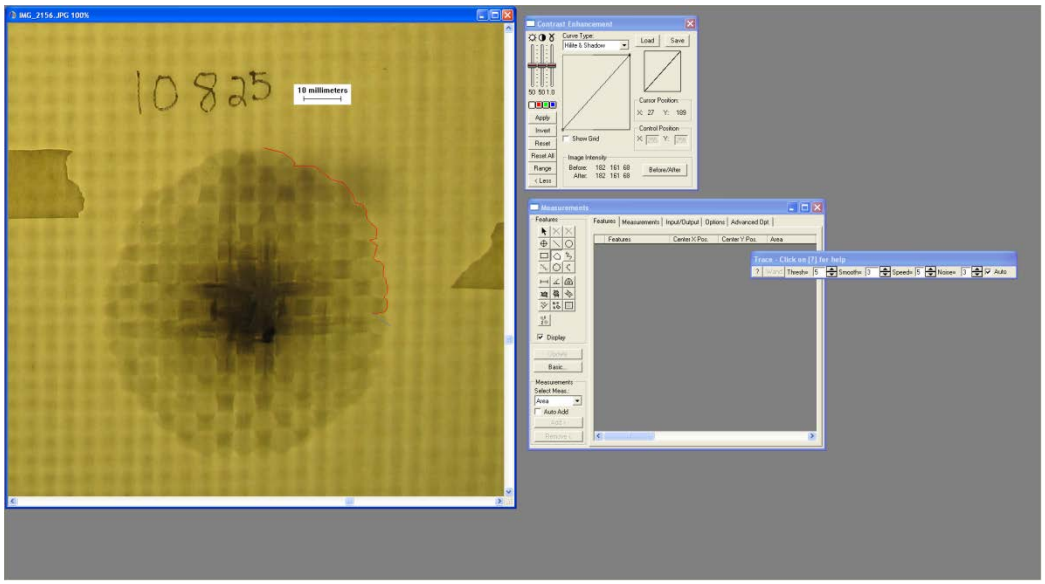

Fig. B-3 Image Pro Plus tools used to outline and measure the delaminations

INTENTIONALLY LEFT BLANK.

Appendix C. Select Post-Impact Images

Figures C-1 through C-4 show delaminations after impact.

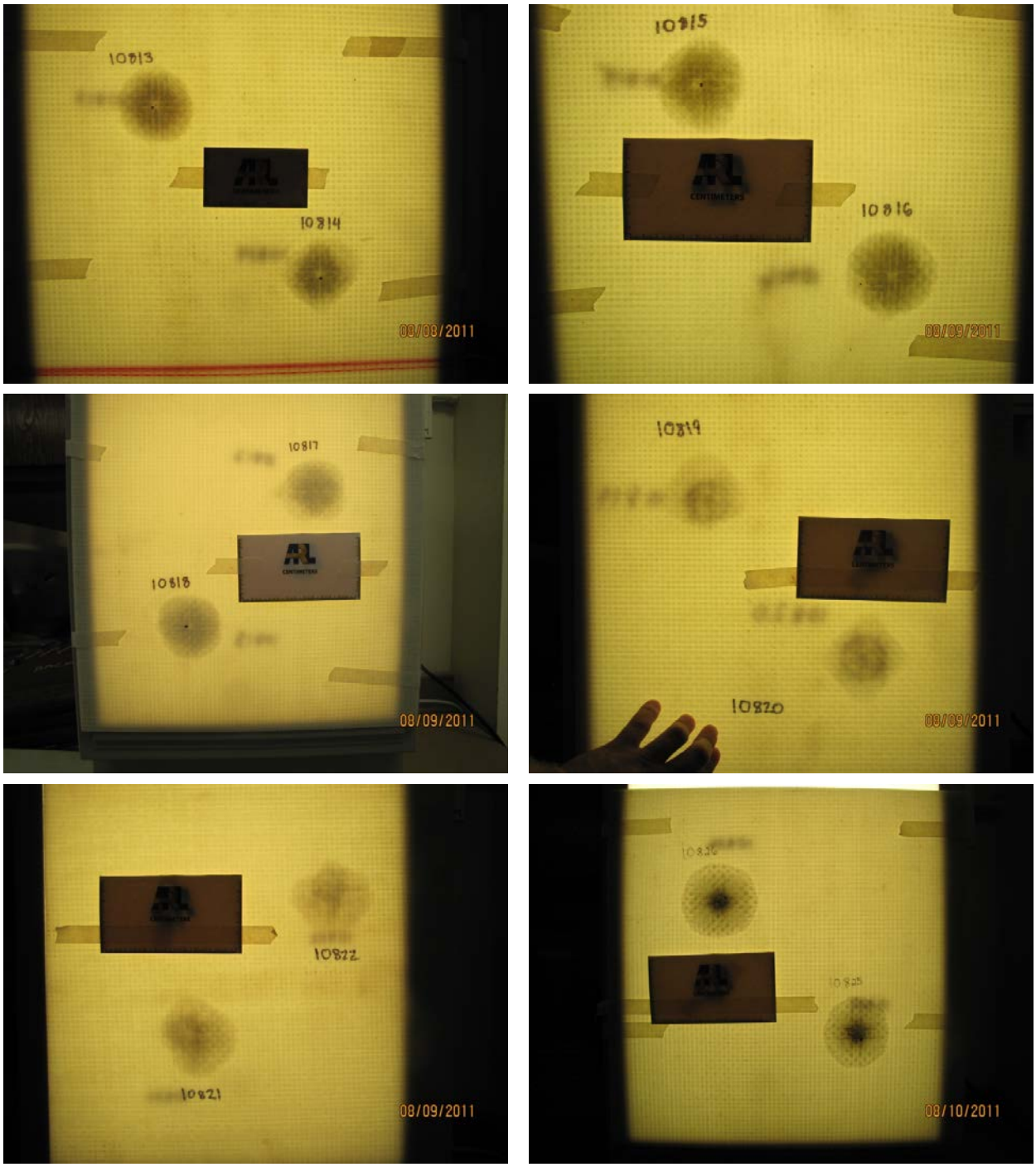

Fig. C-1 Post-impact pictures clearly showing delaminations

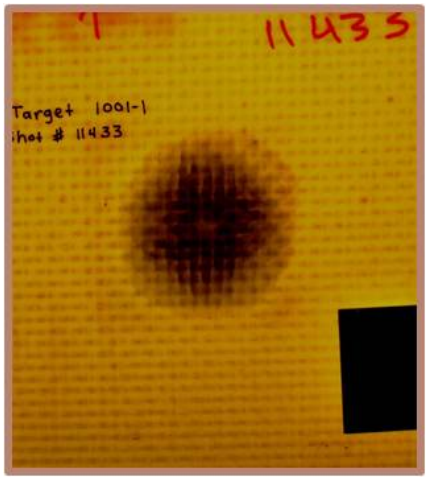

Fig. C-2 Delamination of a center hit

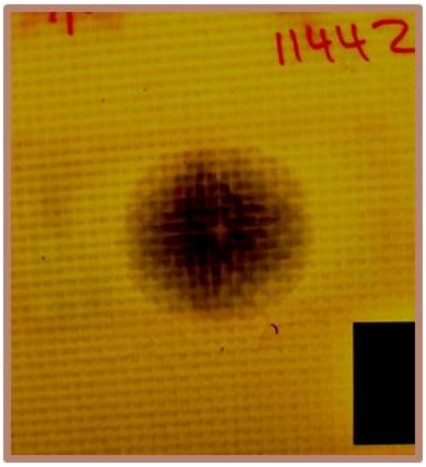

Fig. C-3 Delamination of a 2-tile, seam impact arrangement

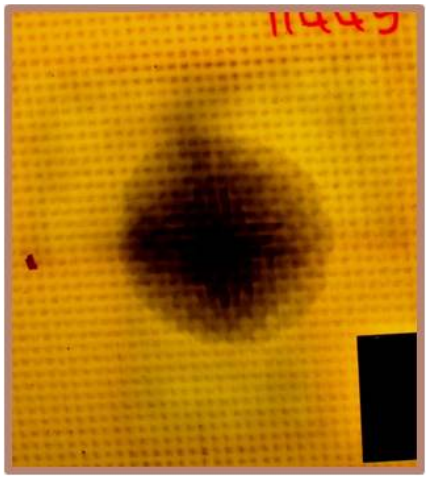

Fig. C-4 Delamination of a 3-tile, triple-point impact arrangement

INTENTIONALLY LEFT BLANK.

Appendix D. Representative Delamination Images for 6-mm-thick, 38.1-mm-diameter Strike Face from the High-Speed Camera

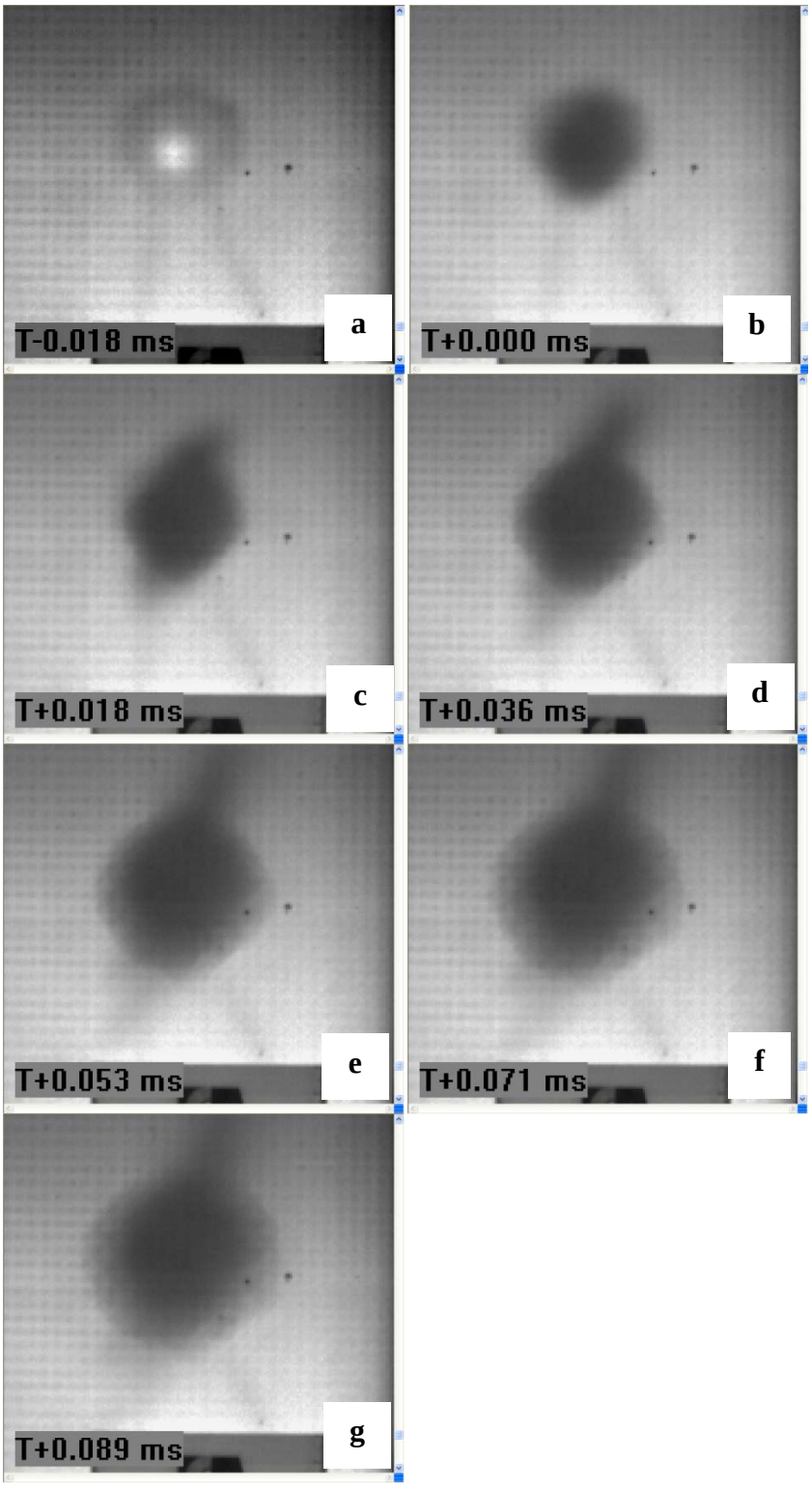

Fig. D-1 Representative sequence of images showing growth of delamination over time (shot 10816, 6-mm-thick, 38.1-mm diameter)

Appendix E. Measuring Velocity Using Phantom Software

Figs. E-1 and E-2 show software imagery measurement

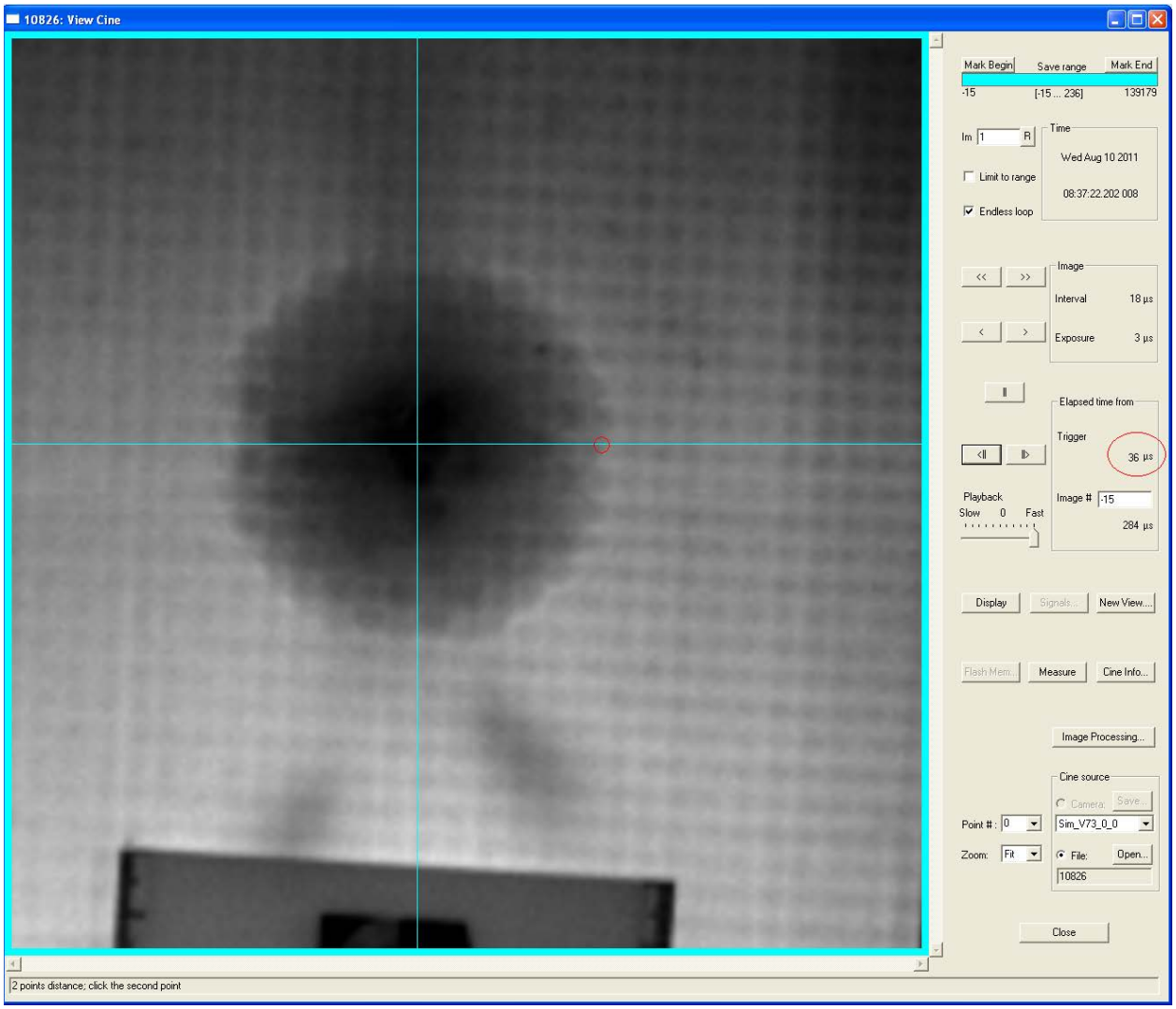

Fig. E-1 Phantom software is used to set a scale to the video. Then 2 points are selected and the software uses the locations and the time (circled) to compute the velocity. The picture is of the first point.

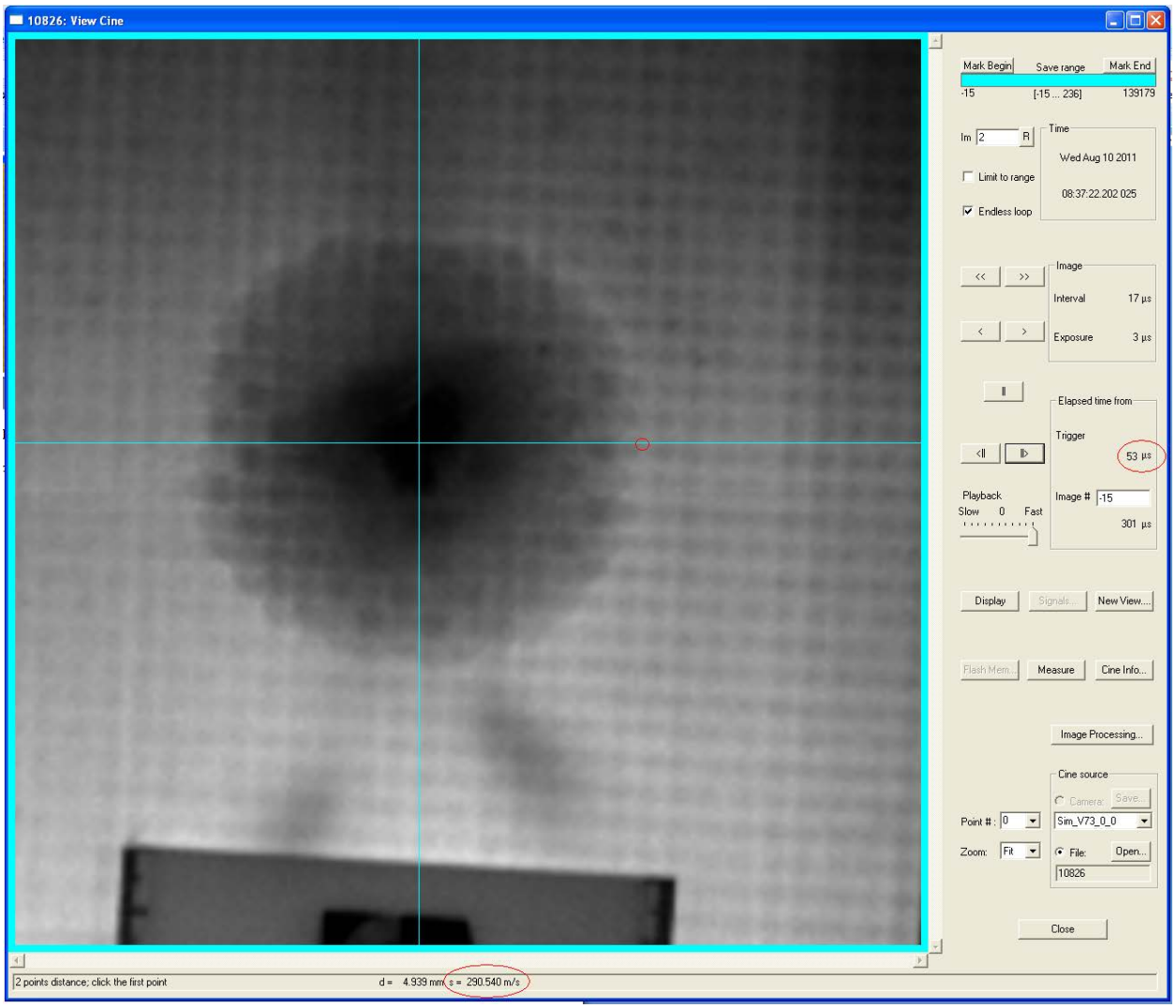

Fig. E-2 Second point that was chosen with point, time, and velocity circled

INTENTIONALLY LEFT BLANK.

Appendix F. Select Velocities Measured

Tables F-1 through F-3 and Figs. F-1 through F-6 detail selected velocity measurements.

Table F-1 Velocity of delamination growth over time for shot 10813, which had a 25.4-mm diameter and was 6 mm thick

Shot No.	Time After Trigger (µs)	Velocity (m/s)
10813 (primary yarns)	33	227
	61	206
	90	28
Average velocity		154
10813 (secondary yarns)	33	173
	61	237
	90	102
Average velocity		154

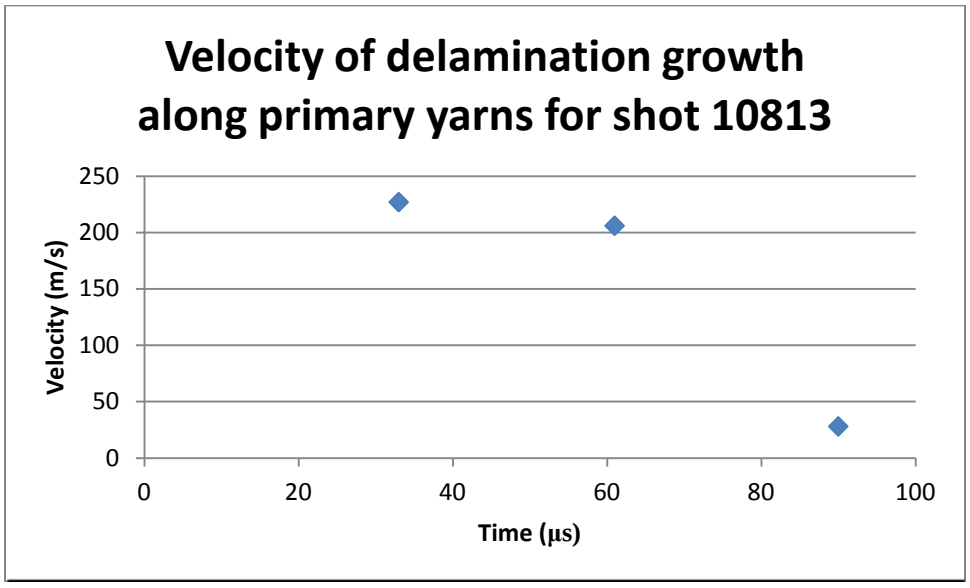

Fig. F-1 Decreasing velocity of the growth of delamination along the primary yarns

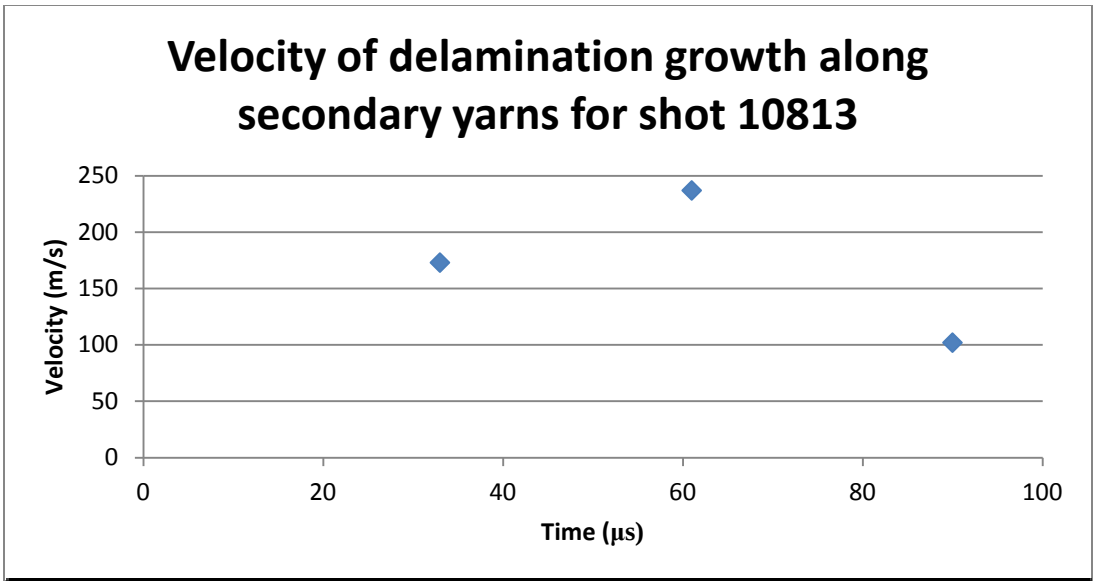

Fig. F-2 Velocities at various times for growth of delamination in the secondary yarns of shot 10813

Table F-2 Velocity of delamination growth over time for shot 10814, which had a 25.4-mm diameter and was 6 mm thick

Shot No.	Time After Trigger (µs)	Velocity (m/s)
10814 (primary yarns)	39	259
	61	222
	83	148
Average velocity		210
10814 (secondary yarns)	39	210
	61	104
	83	52
Average velocity		122

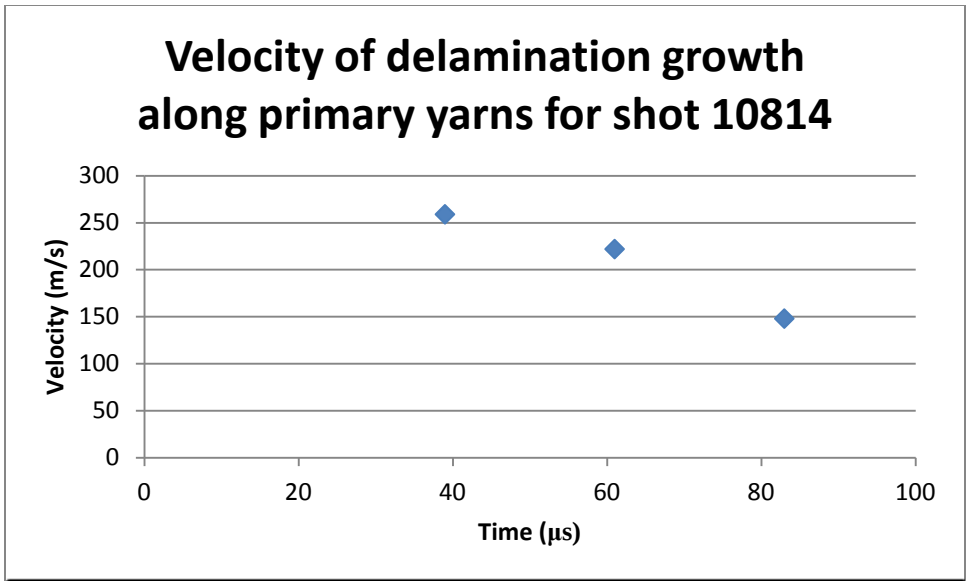

Fig. F-3 Decreasing velocity of delamination growth over time in primary fibers

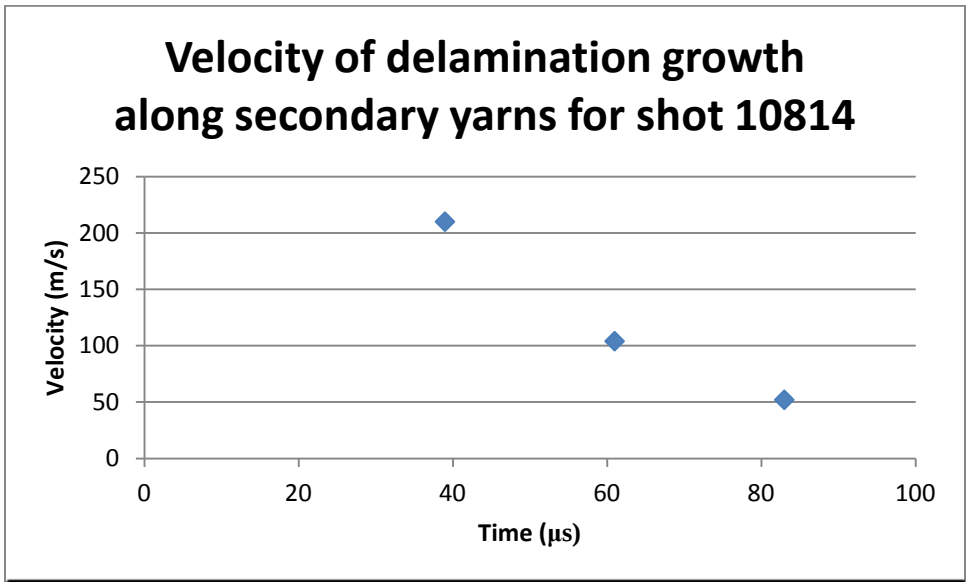

Fig. F-4 Decreasing velocity of delamination growth over time in secondary fibers

Table F-3 Velocity of delamination growth at various times for shot 18018. The glass had a 76.2-mm diameter and was 6 mm thick.

Shot No.	Time (μs)	Velocity (m/s)
10818 (primary yarns)	15	275
	32	242
	50	137
	68	137
	86	92
Average velocity		176.6
10818 (secondary yarns)	15	384
	32	274
	50	495
	68	129
	86	267
Average velocity		307.5

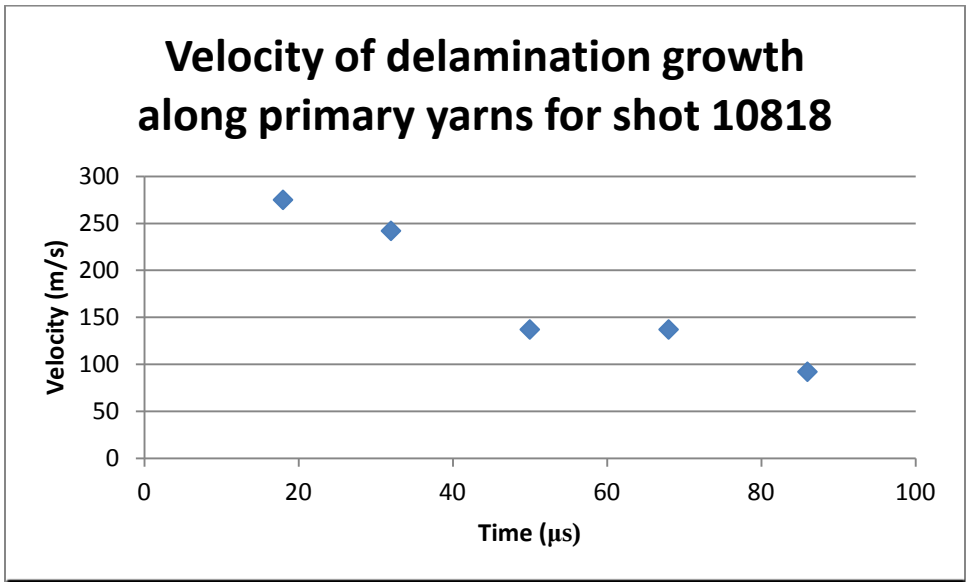

Fig. F-5 Decreasing velocity of delamination growth in primary yarns over time for shot 10818

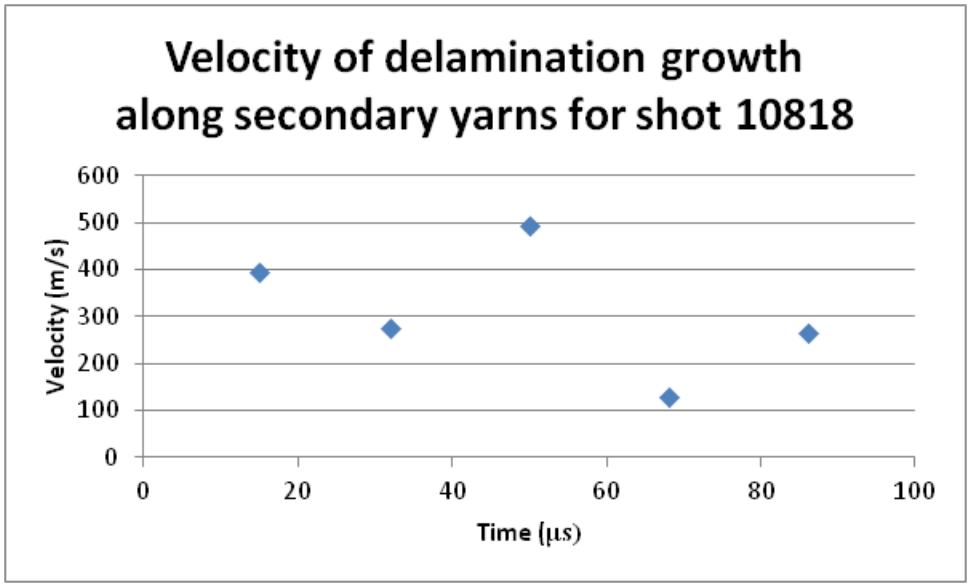

Fig. F-6 Velocities of delamination growth in the secondary yarns at various times for shot 10818

1 (PDF) DEFENSE TECHNICAL INFORMATION CTR DTIC OCA

2 (PDF) DIRECTOR US ARMY RESEARCH LAB RDRL CIO LL IMAL HRA MAIL & RECORDS MGMT

1 (PDF) GOVT PRINTG OFC A MALHOTRA

1 (PDF) COORSTEK VISTA R PALICKA

2 (PDF) SANDIA NATL LABS O ESTRAC J NIEDERHAUS

2 (PDF) SOUTHWEST RSRCH INST J WALKER C ANDERSON

1 (PDF) 3M M NORMANDIA

1 (PDF) DSTL A COOK

48 (PDF) DIR USARL
RDRL LOA
S YOUNG
RDRL WML H
T EHLERS
L MAGNESS
RDRL WMM A
J CAIN
J GARDNER
S GHIORSE
D O'BRIEN
A QUABILI
J SANDS
D SPAGNUOLO
E WETZEL
J WOLBERT
RDRL WMM B
T BOGETTI
S BOYD
R CARTER
B CHEESEMAN
B LOVE
P MOY
A YIOURNAS
RDRL WMM C
R JENSEN
RDRL WMM D
R BRENNAN
L VARGAS
S WALSH
RDRL WMM E
J CAMPBELL
J LASALVIA
P PATEL
J SWAB
T TAYLOR
RDRL WMP B
C HOPPEL
S SATAPATHY
T WEERASOORIYA
RDRL WMP C
T BJERKE
R LEAVY
C WILLIAMS
RDRL WMP E
M BURKINS
B CHAMISH
D CHURN
P DAVIS
D GALLARDY
D HACKBARTH
D HORNBAKER
E HORWATH
J HOUSKAMP
T JONES
M KORNECKI
C KRAUTHAUSER
K MCNAB
P SWOBODA

INTENTIONALLY LEFT BLANK.